A Novel MIMO Car-to-Car Channel Model Based on the Geometrical Curved Street Scattering Model

Nurilla Avazov and Matthias Pätzold
Faculty of Engineering and Science, University of Agder
Servicebox 509, NO-4898 Grimstad, Norway
E-mails: {nurilla.k.avazov, matthias.paetzold}@uia.no

Abstract — **This paper introduces a novel multiple-input multiple-output (MIMO) car-to-car (C2C) channel model, which is based on a geometrical curved street scattering model. Starting from the geometrical model, a MIMO reference channel model is derived under the assumption of a combination of single- and double-bounce scattering in line-of-sight (LOS) and non-LOS (NLOS) propagation environments. The proposed channel model assumes an infinite number of scatterers, which are uniformly distributed on the outer and inner curves of the street. Expressions are presented for the three-dimensional (3D) space-time cross-correlation function (CCF), the temporal autocorrelation function (ACF), and the two-dimensional (2D) space CCF. An efficient sum-of-cisoids (SOC) channel simulator is derived from the reference model. It is shown that the temporal ACF of the SOC channel simulator fits very well to that of the reference model. The validity of the derived reference model has been verified by demonstrating an excellent match between the temporal ACF of the reference model with that of the one-ring model.**

I. Introduction

C2C communication systems are a cornerstone of the envisioned intelligent transportation systems (ITS) [1] because of their key benefits in safety and traveling ease. In C2C communication systems, both the transmitter and the receiver are in motion, which makes the underlying channels different from the traditional fixed-to-mobile or mobile-to-fixed channels in which the base-station is stationary and elevated [2]. For the development of future C2C communication systems, it is necessary to have a detailed knowledge of the statistical properties of the underlying fading channel. Furthermore, C2C communication systems are usually equipped with low elevation antennas. MIMO systems can also be of great benefit for C2C communications due to their higher throughput [3].

In the literature, several MIMO mobile-to-mobile (M2M) channel models have been proposed, such as the one-ring model [4], the two-ring model [5, 6], the elliptical model [7], the T-junction model [8], and the geometrical street model [9]. Simulation models for single-input single-output (SISO) M2M channels have been presented in [10, 11]. A narrowband SISO C2C channel model based on the geometrical street scattering model has been introduced in [9]. A generic and adaptive geometry-based stochastic model for non-isotropic MIMO M2M channels has been proposed in [12], where a combination of single- and double-bounce scattering phenomena have been assumed under LOS propagation conditions. Real-world channel measurements conducted for narrowband and wideband M2M communications have been reported in [13] and [14], respectively. Finally, we mention that 3D reference models for narrowband and wideband MIMO M2M channels have been proposed in [15] and [16], respectively.

In practice, there exist many different street types [17], such as intersections, T-junctions, roundabouts, and U-turns, which have different scattering environments according to their geometry. There are also roads passing through different types of tunnels, which can have the shape of a rectangle or a semi-circle. M. Nilsson *et al.* [18] suggested a simulation model to investigate radio propagation in curved road tunnels at a carrier frequency of 925 MHz. The proposed simulation model rests upon both waveguide methods and geometrical optics. In this paper, we propose a novel geometrical curved street scattering model, which can be used as a starting point for the development of curved, arch, and U-turn street scattering models.

This paper focuses on the statistical characterization of a narrowband reference channel model assuming that an infinite number of scatterers is uniformly distributed on outer and inner curves of the street. The reference model will be derived from the geometrical curved street scattering model assuming that the angle-of-departure (AOD) and the angle-of-arrival (AOA) are dependent in case of single-bounce scattering and independent for the double-bounce scattering components. Moreover, it is assumed that both the mobile transmitter and the mobile receiver are in motion. Expressions of the 3D space-time CCF, the temporal ACF, and the 2D space CCF are derived. The validity of the proposed model is verified by fitting the temporal ACF of the reference model to that of the one-ring model [4]. Furthermore, we derive an SOC channel simulator from the reference model by using the concept [19, Sec. 8.1]. It is shown that the designed channel simulator matches very good the underlying reference model with respect to the temporal ACF.

The rest of this paper is organized as follows. Section II describes the geometrical curved street scattering model. In Section III, the reference channel model is

derived from the geometrical curved street model. Section IV analyzes the correlation properties of the reference model, such as the 3D space-time CCF, the temporal ACF, and the 2D space CCF. Section V describes briefly the simulation model derived from the reference model. The illustration of the numerical results found for the correlation functions of the reference and simulation models are the topic of Section VI. Finally, Section VII draws the conclusions of the paper.

II. The Geometrical Curved Street Scattering Model

In this section, we briefly describe the geometrical curved street scattering model for narrowband MIMO C2C channels shown in Fig. C.1. The proposed geometrical curved street model is the starting point for the derivation of a reference channel model. We assume that the scatterers are uniformly distributed on the outer and the inner curves of the street as illustrated in Fig. C.1. The symbols MS_T and MS_R in Fig. C.1 stand for the mobile transmitter and the mobile receiver, respectively. With regard to MS_T, we suppose that there are M_p scatterers located on the outer

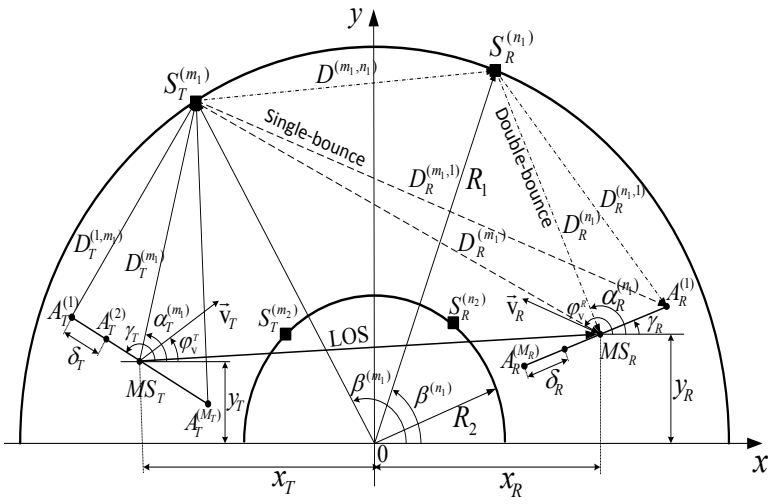

Figure C.1: Geometrical curved street scattering model with single-bounce ($- - -$), double-bounce ($-\cdot-$), and LOS (—-) components for MIMO C2C channels.

$(p=1)$ and the inner $(p=2)$ semi-circles with radii R_1 and R_2, where the m_pth $(m_p = 1,2,\ldots,M_p)$ effective scatterer is denoted by $S_T^{(m_p)}$. Analogously, with regard to MS_R, we assume that there are N_q scatterers located on the outer $(q=1)$ and the inner $(q=2)$ semi-circles with radii R_1 and (R_2), where the n_qth $(n_q = 1,2,\ldots,N_q)$ effective scatterer is denoted by $S_R^{(n_q)}$. The symbol $\beta^{(m_p)}$ $(\beta^{(n_q)})$ denotes the angle-of-scatterer (AOS) associated with the scatterer $S_T^{(m_p)}$ $(S_R^{(n_q)})$. The transmitter (receiver) is located at the position x_T and y_T (x_R and y_R). Both the transmitter and the receiver are in motion and equipped with M_T transmitter antenna elements and M_R

receiver antenna elements, respectively. The antenna element spacings at the transmitter and the receiver are denoted by δ_T and δ_R, respectively. The symbols $\alpha_T^{(m_p)}$ and $\alpha_R^{(n_q)}$ denote the AOD and the AOA, respectively. The angle γ_T (γ_R) describes the tilt angle of the transmitter (receiver) antenna array. Furthermore, it is assumed that the transmitter (receiver) moves with speed v_T (v_R) in the direction determined by the angle-of-motion φ_{v}^T (φ_{v}^R).

III. The Reference Model

This section presents the reference model for the MIMO C2C channel by considering a combination of single- and double-bounce scattering under the assumption of LOS and NLOS propagation conditions shown in Fig. C.1. From Fig. C.1, we can observe that the complex channel gain $g_{kl}(t)$ of the link between the lth transmitter antenna element $A_T^{(l)}$ ($l = 1,2,\ldots,M_T$) and the kth receiver antenna element $A_R^{(k)}$ ($k = 1,2,\ldots,M_R$) can be expressed as a superposition of single-bounce, double-bounce, and LOS components as follows

$$g_{kl}(t) = g_{kl}^{\mathrm{SB}}(t) + g_{kl}^{\mathrm{DB}}(t) + g_{kl}^{\mathrm{LOS}}(t) \tag{C.1}$$

where $g_{kl}^{\mathrm{SB}}(t)$, $g_{kl}^{\mathrm{DB}}(t)$ and $g_{kl}^{\mathrm{LOS}}(t)$ denote the single-bounce, the double-bounce, and the LOS components of the complex channel gain $g_{kl}(t)$, respectively.

A. Derivation of the Double-Bounce Scattering Component

In this subsection, we derive the double-bounce scattering component $g_{kl}^{\mathrm{DB}}(t)$ of the complex channel gain. As shown in Fig. C.1, we realize that the m_pth homogeneous plane wave emitted from the lth antenna element $A_T^{(l)}$ of the transmitter travels over the local scatterers $S_T^{(m_p)}$ and $S_R^{(n_q)}$ on the outer ($p = q = 1$) and the inner ($p = q = 2$) semi-circles before impinging on the kth antenna element $A_R^{(k)}$ of the receiver. The reference model is based on the assumption that the number of local scatterers on the outer and the inner semi-circles are infinite, i.e., $M_p, N_q \to \infty$. Under the flat-fading channel assumption, the double-bounce scattering component $g_{kl}^{\mathrm{DB}}(t)$ of the link between the lth transmitter antenna element $A_T^{(l)}$ and the kth receiver antenna element $A_R^{(k)}$ can be expressed as a superposition of the double-bounce scattering components from the outer and the inner semi-circles

$$g_{kl}^{\mathrm{DB}}(t) \;=\; \sum_{p,q=1}^{2} g_{kl}^{\mathrm{DB},p,q}(t) \tag{C.2}$$

where

$$g_{kl}^{\mathrm{DB},p,q}(t) = \lim_{M_p,N_q\to\infty} \frac{1}{\sqrt{(c_R+1)M_pN_q}} \sum_{m_p,n_q=1}^{M_p,N_q} a_l^{(m_p)} b_k^{(n_q)} c_{m_pn_q} \cdot e^{j\left[2\pi\left(f_T^{(m_p)}+f_R^{(nq)}\right)t+\theta_{m_pn_q}\right]} \tag{C.3}$$

and

$$a_l^{(m_p)} = e^{j\pi(\delta_T/\lambda)(M_T-2l+1)\cos\left(\alpha_T^{(m_p)}-\gamma_T\right)} \tag{C.4}$$

$$b_k^{(n_q)} = e^{j\pi(\delta_R/\lambda)(M_R-2k+1)\cos\left(\alpha_R^{(nq)}-\gamma_R\right)} \tag{C.5}$$

$$c_{m_pn_q} = e^{-j\frac{2\pi}{\lambda}\left(D_T^{(m_p)}+D_R^{(nq)}\right)} \tag{C.6}$$

$$f_T^{(m_p)} = f_{T\max}\cos\left(\alpha_T^{(m_p)}-\varphi_{\mathrm{v}}^T\right) \tag{C.7}$$

$$f_R^{(n_q)} = f_{R\max}\cos\left(\alpha_R^{(n_q)}-\varphi_{\mathrm{v}}^R\right). \tag{C.8}$$

In (C.7) and (C.8), the symbols $f_{T\max} = \mathrm{v}_T/\lambda$ and $f_{R\max} = \mathrm{v}_R/\lambda$ denote the maximum Doppler frequencies, and λ is the wavelength. The symbol c_R in (C.3) represents the Rice factor, which is defined as the ratio of the power of the LOS component to the power of the sum of single- and double-bounce components, i.e., $c_R = E\{|g_{kl}^{\mathrm{LOS}}(t)|^2\}/E\{|g_{kl}^{\mathrm{SB}}(t)+g_{kl}^{\mathrm{DB}}(t)|^2\}$. In our model, we assume that the scatterers $S_T^{(m_p)}$ and $S_R^{(n_q)}$ introduce the phase shifts θ_{m_p} and θ_{n_q}, respectively. The phase shifts θ_{m_p} and θ_{n_q} are assumed to be independent, identically distributed (i.i.d.) random variables, which are uniformly distributed over the interval $[0,2\pi)$. Hence, the joint phase $\theta_{m_pn_q}$ in (C.3) can be expressed in the following form [5]

$$\theta_{m_pn_q} = \theta_{m_p}+\theta_{n_q}. \tag{C.9}$$

B. Derivation of the Single-Bounce Scattering Component

In Fig. C.1, the single-bounce scattering path from the scatterer $S_T^{(m_p)}$ to the kth antenna element $A_R^{(k)}$ of the receiver is denoted by a dashed line. In case of single-bounce scattering, the m_pth homogeneous plane wave emitted from the lth antenna element $A_T^{(l)}$ of the transmitter travels over the local scatterer $S_T^{(m_p)}$ before impinging on the kth antenna element $A_R^{(k)}$ of the receiver. Hence, the single-bounce scattering component of the complex channel gain $g_{kl}^{\mathrm{SB}}(t)$ can be obtained by considering only

the effective scatterers $S_T^{(m_p)}$ [see Fig. C.1], for $n_q = m_p$ and $q = p$, as

$$g_{kl}^{\mathrm{SB}}(t) = \sum_{p=1}^{2} \lim_{M_p \to \infty} \frac{1}{\sqrt{(c_R+1)M_p}} \sum_{m_p=1}^{M_p} a_l^{(m_p)} b_k^{(m_p)} c_{m_p} \cdot e^{j\left[2\pi\left(f_T^{(m_p)} + f_R^{(m_p)}\right)t + \theta_{m_p}\right]} \tag{C.10}$$

where

$$a_l^{(m_p)} = e^{j\pi(\delta_T/\lambda)(M_T-2l+1)\cos\left(\alpha_T^{(m_p)}-\gamma_T\right)} \tag{C.11}$$

$$b_k^{(m_p)} = e^{j\pi(\delta_R/\lambda)(M_R-2k+1)\cos\left(\alpha_R^{(m_p)}-\gamma_R\right)} \tag{C.12}$$

$$c_{m_p} = e^{-j\frac{2\pi}{\lambda}\left(D_T^{(m_p)}+D_R^{(m_p)}\right)} \tag{C.13}$$

$$f_T^{(m_p)} = f_{T_{\max}} \cos\left(\alpha_T^{(m_p)} - \varphi_{\mathrm{v}}^T\right) \tag{C.14}$$

$$f_R^{(m_p)} = f_{R_{\max}} \cos\left(\alpha_R^{(m_p)} - \varphi_{\mathrm{v}}^R\right). \tag{C.15}$$

C. The LOS Component

The LOS component $g_{kl}^{\mathrm{LOS}}(t)$ in (C.1) is given by

$$g_{kl}^{\mathrm{LOS}}(t) = \sqrt{\frac{c_R}{(c_R+1)}} a_l^{(0)} b_k^{(0)} c^{(0)} e^{j2\pi\left(f_T^{(0)}+f_R^{(0)}\right)t} \tag{C.16}$$

where

$$a_l^{(0)} = e^{j\pi(\delta_T/\lambda)(M_T-2l+1)\cos(\gamma_T)} \tag{C.17}$$

$$b_k^{(0)} = e^{-j\pi(\delta_R/\lambda)(M_R-2k+1)\cos(\gamma_R)} \tag{C.18}$$

$$c^{(0)} = e^{-j\frac{2\pi}{\lambda}\sqrt{(y_R-y_T)^2+(x_T+x_R)^2}} \tag{C.19}$$

$$f_T^{(0)} = f_{T_{\max}} \cos\left(\alpha_T^{(0)} - \varphi_{\mathrm{v}}^T\right) \tag{C.20}$$

$$f_R^{(0)} = f_{R_{\max}} \cos\left(\alpha_R^{(0)} - \varphi_{\mathrm{v}}^R\right). \tag{C.21}$$

In (C.16), $f_T^{(0)}$ and $f_R^{(0)}$ denote the Doppler shifts of the LOS component caused by the movement of the transmitter and the receiver, respectively. The symbols $\alpha_T^{(0)}$ and $\alpha_R^{(0)}$ in (C.20) and (C.21), respectively, represent the AOD and the AOA of the LOS component.

D. Derivation of the AOD and the AOA

The position of all local scatterers $S_T^{(m_p)}$ and $S_R^{(n_q)}$ is described by the AOSs $\beta^{(m_p)}$ and $\beta^{(n_q)}$, respectively. With reference to Fig. C.1 and by using elementary

trigonometric identities, we can express the relationships between the AOD $\alpha_T^{(m_p)}$ and the AOS $\beta^{(m_p)}$ as well as between the AOA $\alpha_R^{(n_q)}$ and the AOS $\beta^{(n_q)}$. Hence, by using the following two functions

$$g_T(\beta^{(m_p)}) = \arctan\left(\frac{\frac{R_p}{\sqrt{x_T^2+y_T^2}}\sin\beta^{(m_p)} - \sin\alpha_T'}{\cos\alpha_T' + \frac{R_p}{\sqrt{x_T^2+y_T^2}}\cos\beta^{(m_p)}}\right) \tag{C.22}$$

$$g_R(\beta^{(n_q)}) = \arctan\left(\frac{\frac{R_q}{\sqrt{x_R^2+y_R^2}}\sin\beta^{(n_q)} - \sin\alpha_R'}{\frac{R_q}{\sqrt{x_R^2+y_R^2}}\cos\beta^{(n_q)} - \cos\alpha_R'}\right) \tag{C.23}$$

where $\alpha_T' = \arctan(y_T/x_T)$ and $\alpha_R' = \arctan(y_R/x_R)$, we can express the AOD $\alpha_T^{(m_p)}(\beta^{(m_p)})$ and the AOA $\alpha_R^{(n_q)}(\beta^{(n_q)})$ for the outer ($p=q=1$) and the inner ($p=q=2$) semi-circles as follows:

1) Outer semi-circle

$$\alpha_T^{(m_1)}(\beta^{(m_1)}) = \begin{cases} g_T(\beta^{(m_1)}), & \text{if} \quad 0 \le \beta^{(m_1)} \le \pi - \arccos(\frac{x_T}{R_1}) \\ \pi + g_T(\beta^{(m_1)}), & \text{if} \quad \pi - \arccos(\frac{x_T}{R_1}) < \beta^{(m_1)} \le \pi \end{cases} \tag{C.24}$$

$$\alpha_R^{(n_1)}(\beta^{(n_1)}) = \begin{cases} g_R(\beta^{(n_1)}), & \text{if} \quad 0 \le \beta^{(n_1)} \le \arccos(\frac{x_R}{R_1}) \\ \pi + g_R(\beta^{(n_1)}), & \text{if} \quad \arccos(\frac{x_R}{R_1}) < \beta^{(n_1)} \le \pi\,. \end{cases} \tag{C.25}$$

2) Inner semi-circle

$$\begin{aligned} \alpha_T^{(m_2)}(\beta^{(m_2)}) &= g_T(\beta^{(m_2)}), \quad \text{if } 0 \le \beta^{(m_2)} \le \pi \\ \alpha_R^{(n_2)}(\beta^{(n_2)}) &= \pi + g_R(\beta^{(n_2)}), \text{ if } 0 \le \beta^{(n_2)} \le \pi\,. \end{aligned} \tag{C.26}$$

(C.27)

IV. Correlation Properties of the Reference Model

In this section, we derive a general analytical solution for the 3D space-time CCF from which other correlation functions, such as the temporal ACF and the 2D space CCF can easily be derived.

A. Derivation of the 3D Space-Time CCF

According to [2], the 3D space-time CCF of the links $A_T^{(l)} - A_R^{(k)}$ and $A_T^{(l')} - A_R^{(k')}$ is defined as the correlation between the complex channel gains $g_{kl}(t)$ and $g_{k'l'}(t)$, i.e.,

$$\begin{aligned} \rho_{kl,k'l'}(\delta_T,\delta_R,\tau) &:= E\{g_{kl}^*(t)g_{k'l'}(t+\tau)\} \\ &= \rho_{kl,k'l'}^{\mathrm{SB}}(\delta_T,\delta_R,\tau)+\rho_{kl,k'l'}^{\mathrm{DB}}(\delta_T,\delta_R,\tau) \\ &\quad +\rho_{kl,k'l'}^{\mathrm{LOS}}(\delta_T,\delta_R,\tau) \end{aligned} \tag{C.28}$$

where $(*)$ denotes the complex conjugate operator, and $E\{\cdot\}$ stands for the expectation operator that applies to all random variables, namely the phases $\theta_{m_p n_q}$ and the AOSs $\beta^{(m_p)}$ and $\beta^{(n_q)}$. The symbols $\rho_{kl,k'l'}^{\mathrm{SB}}(\delta_T,\delta_R,\tau)$, $\rho_{kl,k'l'}^{\mathrm{DB}}(\delta_T,\delta_R,\tau)$, and $\rho_{kl,k'l'}^{\mathrm{LOS}}(\delta_T,\delta_R,\tau)$ represent the 3D space-time CCF of the single-bounce, the double-bounce, and LOS components, respectively.

The 3D space-time CCF $\rho_{kl,k'l'}^{\mathrm{DB}}(\delta_T,\delta_R,\tau)$ of the double-bounce scattering component $g_{k,l}^{\mathrm{DB}}(t)$ is given by

$$\rho_{kl,k'l'}^{\mathrm{DB}}(\delta_T,\delta_R,\tau) = \sum_{p,q=1}^{2} \rho_{kl,k'l'}^{\mathrm{DB},p,q}(\delta_T,\delta_R,\tau) \tag{C.29}$$

where

$$\begin{aligned} \rho_{kl,k'l'}^{\mathrm{DB},p,q}(\delta_T,\delta_R,\tau) = \lim_{M_pN_q\to\infty} \frac{1}{(c_R+1)M_pN_q} \sum_{m_p,n_q=1}^{M_p,N_q} E\Big\{ c_{ll'}^{(m_p)} d_{kk'}^{(n_q)} \\ \cdot e^{j2\pi\left(f_T^{(m_p)}+f_R^{(n_q)}\right)\tau} \Big\} \end{aligned} \tag{C.30}$$

and

$$c_{ll'}^{(m_p)} = e^{j2\pi(\delta_T/\lambda)(l-l')\cos\left(\alpha_T^{(m_p)}-\gamma_T\right)} \tag{C.31}$$

$$d_{kk'}^{(n_q)} = e^{j2\pi(\delta_R/\lambda)(k-k')\cos\left(\alpha_R^{(n_q)}-\gamma_R\right)}. \tag{C.32}$$

The quantities $f_T^{(m_p)}$ and $f_R^{(n_q)}$ are given by (C.7) and (C.8), respectively. We recall that the AOD $\alpha_T^{(m_p)}$ and the AOA $\alpha_R^{(n_q)}$ can be expressed in terms of the random variables $\beta^{(m_p)}$ and $\beta^{(n_q)}$ by using (C.22) and (C.23), respectively.

The 3D space-time CCF $\rho^{\mathrm{SB}}_{kl,k'l'}(\delta_T,\delta_R,\tau)$ of the single-bounce scattering component $g^{\mathrm{SB}}_{k,l}(t)$ can be obtained by considering only the effective scatterers $S^{(m_p)}$, for $n_q = m_p$ and $q = p$, as

$$\begin{aligned}\rho^{\mathrm{SB}}_{kl,k'l'}(\delta_T,\delta_R,\tau) \;=\; \sum_{p=1}^{2} \lim_{M_p\to\infty} \frac{1}{(c_R+1)M_p} \sum_{m_p=1}^{M_p} E\Big\{ c_{ll'}^{(m_p)} d_{kk'}^{(m_p)} \\ \cdot e^{j2\pi\left(f_T^{(m_p)}+f_R^{(m_p)}\right)\tau}\Big\}\end{aligned} \tag{C.33}$$

where

$$c_{ll'}^{(m_p)} \;=\; e^{j2\pi(\delta_T/\lambda)(l-l')\cos\left(\alpha_T^{(m_p)}-\gamma_T\right)} \tag{C.34}$$

$$d_{kk'}^{(m_p)} \;=\; e^{j2\pi(\delta_R/\lambda)(k-k')\cos\left(\alpha_R^{(m_p)}-\gamma_R\right)}. \tag{C.35}$$

The Doppler frequencies $f_T^{(m_p)}$ and $f_R^{(m_p)}$ are given by (C.14) and (C.15), respectively.

In Section II, it has been mentioned that all scatterers are uniformly distributed on the outer and inner semi-circles [see Fig. C.1]. Hence, the random variables $\beta^{(m_p)}$ and $\beta^{(n_q)}$ are also uniformly distributed over the intervals $[\beta^{(p)}_{\min},\beta^{(p)}_{\max}]$ and $[\beta^{(q)}_{\min},\beta^{(q)}_{\max}]$, respectively. If the number of scatterers tends to infinity, i.e., $M_p, N_q \to \infty$, then the discrete random variables $\beta^{(m_p)}$ and $\beta^{(n_q)}$ become continuous random variables denoted by $\beta^{(p)}$ and $\beta^{(q)}$, respectively. Thus, the probability density functions (PDFs) $p_{\beta^{(p)}}(\beta^{(p)})$ and $p_{\beta^{(q)}}(\beta^{(q)})$ of $\beta^{(p)}$ and $\beta^{(q)}$, respectively, are given by

$$p_{\beta^{(p)}}(\beta^{(p)}) \;=\; \frac{1}{\beta^{(p)}_{\max}-\beta^{(p)}_{\min}}, \quad \beta^{(p)} \in [\beta^{(p)}_{\min},\beta^{(p)}_{\max}] \tag{C.36}$$

$$p_{\beta^{(q)}}(\beta^{(q)}) \;=\; \frac{1}{\beta^{(q)}_{\max}-\beta^{(q)}_{\min}}, \quad \beta^{(q)} \in [\beta^{(q)}_{\min},\beta^{(q)}_{\max}]. \tag{C.37}$$

The infinitesimal power of the diffuse component corresponding to the differential angles $d\beta^{(p)}$ and $d\beta^{(q)}$ is proportional to $p_{\beta^{(p)}}(\beta^{(p)})p_{\beta^{(q)}}(\beta^{(q)})d\beta^{(p)}d\beta^{(q)}$. As $M_p, N_q \to \infty$, this infinitesimal contribution must be equal to $1/(M_pN_q) = p_{\beta^{(p)}}(\beta^{(p)})p_{\beta^{(q)}}(\beta^{(q)})d\beta^{(p)}d\beta^{(q)}$. Consequently, it follows that (C.30) can be ex-

pressed as

$$\rho^{\mathrm{DB},p,q}_{kl,k'l'}(\delta_T,\delta_R,\tau) = \frac{1}{(c_R+1)}\int_{\beta^{(p)}_{\min}}^{\beta^{(p)}_{\max}}\int_{\beta^{(q)}_{\min}}^{\beta^{(q)}_{\max}} c^{(p)}_{ll'}(\delta_T,\beta^{(p)})d^{(q)}_{kk'}(\delta_R,\beta^{(q)}) \cdot e^{j2\pi\left(f^{(p)}_T(\beta^{(p)})+f^{(q)}_R(\beta^{(q)})\right)\tau} p_{\beta^{(p)}}(\beta^{(p)}) \cdot p_{\beta^{(q)}}(\beta^{(q)})d\beta^{(p)}d\beta^{(q)} \quad \text{(C.38)}$$

where

$$c^{(p)}_{ll'}(\delta_T,\beta^{(p)}) = e^{j2\pi\frac{\delta_T}{\lambda}(l-l')\cos\left(\alpha_T(\beta^{(p)})-\gamma_T\right)} \quad \text{(C.39)}$$

$$d^{(q)}_{kk'}(\delta_R,\beta^{(q)}) = e^{j2\pi\frac{\delta_R}{\lambda}(k-k')\cos\left(\alpha_R(\beta^{(q)})-\gamma_R\right)} \quad \text{(C.40)}$$

$$f^{(p)}_T(\beta^{(p)}) = f_{T_{\max}}\cos\left(\alpha^{(p)}_T(\beta^{(p)})-\varphi^T_{\mathrm{v}}\right) \quad \text{(C.41)}$$

$$f^{(q)}_R(\beta^{(q)}) = f_{R_{\max}}\cos\left(\alpha^{(q)}_R(\beta^{(q)})-\varphi^R_{\mathrm{v}}\right). \quad \text{(C.42)}$$

In (C.41) and (C.42), we recall that the AOD $\alpha^{(p)}_T(\beta^{(p)})$ and the AOA $\alpha^{(q)}_R(\beta^{(q)})$ are functions of the AOSs $\beta^{(p)}$ and $\beta^{(q)}$ according to (C.24)–(C.27). Thus, after substituting (C.38) in (C.29), we can express the 3D space-time CCF of the double-bounce scattering component in integral form.

The 3D space-time CCF of the single-bounce scattering component is given by

$$\rho^{\mathrm{SB}}_{kl,k'l'}(\delta_T,\delta_R,\tau) = \frac{1}{(c_R+1)}\sum_{p=1}^{2}\int_{\beta^{(p)}_{\min}}^{\beta^{(p)}_{\max}} c^{(p)}_{ll'}(\delta_T,\beta^{(p)})d^{(p)}_{kk'}(\delta_R,\beta^{(p)}) \cdot e^{j2\pi\left(f^{(p)}_T(\beta^{(p)})+f^{(p)}_R(\beta^{(p)})\right)\tau} p_{\beta^{(p)}}(\beta^{(p)})d\beta^{(p)}. \quad \text{(C.43)}$$

Finally, the 3D space-time CCF $\rho^{\mathrm{LOS}}_{kl,k'l'}(\delta_T,\delta_R,\tau)$ of the LOS component $g^{\mathrm{LOS}}_{kl}(t)$ is obtained as

$$\rho^{\mathrm{LOS}}_{kl,k'l'}(\delta_T,\delta_R,\tau) = \frac{c_R}{(c_R+1)}c^{(0)}_{ll'}(\delta_T)d^{(0)}_{kk'}(\delta_R)e^{j2\pi\left(f^{(0)}_T+f^{(0)}_R\right)\tau} \quad \text{(C.44)}$$

where

$$c^{(0)}_{ll'}(\delta_T) = e^{j2\pi(\delta_T/\lambda)(l-l')\cos(\gamma_T)} \quad \text{(C.45)}$$

$$d^{(0)}_{kk'}(\delta_R) = e^{-j2\pi(\delta_R/\lambda)(k-k')\cos(\gamma_R)}. \quad \text{(C.46)}$$

The Doppler shifts $f_T^{(0)}$ and $f_R^{(0)}$ are given by (C.20) and (C.21), respectively.

B. The 2D Space CCF

The 2D space CCF $\rho_{kl,k'l'}(\delta_T,\delta_R)$ is defined as $\rho_{kl,k'l'}(\delta_T,\delta_R) := E\{g_{kl}^*(t)g_{k'l'}(t)\}$, which equals the 3D space-time CCF $\rho_{kl,k'l'}(\delta_T,\delta_R,\tau)$ at $\tau = 0$, i.e.,

$$\begin{aligned}\rho_{kl,k'l'}(\delta_T,\delta_R) &= \rho_{kl,k'l'}^{\mathrm{SB}}(\delta_T,\delta_R,0)+\rho_{kl,k'l'}^{\mathrm{DB}}(\delta_T,\delta_R,0)\\ &\quad +\rho_{kl,k'l'}^{\mathrm{LOS}}(\delta_T,\delta_R,0)\,. \end{aligned} \tag{C.47}$$

C. The Temporal ACF

The temporal ACF of the complex channel gain $g_{kl}(t)$ of the transmission link from $A_T^{(l)}$ $(l = 1,2,\ldots,M_T)$ to $A_R^{(k)}$ $(k = 1,2,\ldots,M_R)$ is defined by $r_{g_{kl}}(\tau) := E\{g_{kl}^*(t)g_{kl}(t+\tau)\}$ [20, p. 376]. The temporal ACF can directly be obtained from the 3D space-time CCF [see (C.28)] by setting the antenna element spacings δ_T and δ_R to zero. By using (C.29), (C.38), (C.43), and (C.44), this results in

$$\begin{aligned}r_{g_{kl}}(\tau) &= \rho_{kl,k'l'}^{\mathrm{SB}}(0,0,\tau)+\rho_{kl,k'l'}^{\mathrm{DB}}(0,0,\tau)\\ &\quad +\rho_{kl,k'l'}^{\mathrm{LOS}}(0,0,\tau)\,. \end{aligned} \tag{C.48}$$

V. The Simulation Model

The reference model described above can serve as basis for the derivation of stochastic and deterministic simulation models [19, Sec. 8.1]. In the literature, a large number of models exist that allow for a proper simulation of mobile channels. The SOC model is an appropriate simulation model for mobile radio channels under non-isotropic scattering conditions. A detailed description and design concept of SOC models can be found in [21] and [22], respectively. For our model, we use the L_p-norm method (LPNM) [19, Sec. 5.4.3], which is a high-performance parameter computation method for the design of SOC channel simulators.

VI. Performance Evaluation

This section illustrates the results in (C.47) and (C.48). The performance of the channel simulator has been assessed by comparison of its temporal ACF to that of the reference model in (C.48). As our geometrical curved street scattering model, we consider semi-circles with radii $R_1 = 14$ m and $R_2 = 8$ m for the outer and the inner semi-circles, respectively. With reference to Fig. C.1, the positions of the transmitter and the receiver are defined by the distances $(x_T, y_T) = (10\text{ m}, 2\text{ m})$, and $(x_R, y_R) = (12\text{ m}, 4\text{ m})$, respectively. For the reference model, all theoretical results have been obtained by choosing the following parameters: $\gamma_T = 90^\circ$, $\gamma_R = 90^\circ$,

$\varphi_{\mathrm{v}}^{T} = 90^{\circ}$, $\varphi_{\mathrm{v}}^{R} = 90^{\circ}$, $\beta^{(p)} \in [0, 180^{\circ}]$ $(p = 1,2)$, $\beta^{(q)} \in [0, 180^{\circ}]$ $(q = 1,2)$, and $f_{T_{\max}} = f_{R_{\max}} = 91$ Hz. The Rice factor c_R was chosen from the set $\{0, 0.5, 1\}$. The scatterers are uniformly distributed on semi-circles. The L_p-norm method [19, Sec. 5.4.3] has been used to optimize the simulation model parameters by assuming a finite number of scatterers (cisoids). For the simulation model, we use $M_1 = N_1 = 50$ scatterers (cisoids) on the outer semi-circle and $M_2 = N_2 = 50$ on the inner semi-circle.

Fig. C.2 illustrates the absolute value of the temporal ACF $|r_{g_{11}}(\tau)|$ for the case that both the transmitter and the receiver are moving towards each other. A good fitting between the temporal ACF of the reference model and that of the simulation model can be observed. This figure demonstrates also that the experimental simulation results of the temporal ACF match very well with the theoretical results. From Fig. C.2, we can observe that the approximation error caused by a limited number of scatterers (cisoids) M_p, N_q can in general be ignored if $M_p \geq 50$ and $N_q \geq 50$.

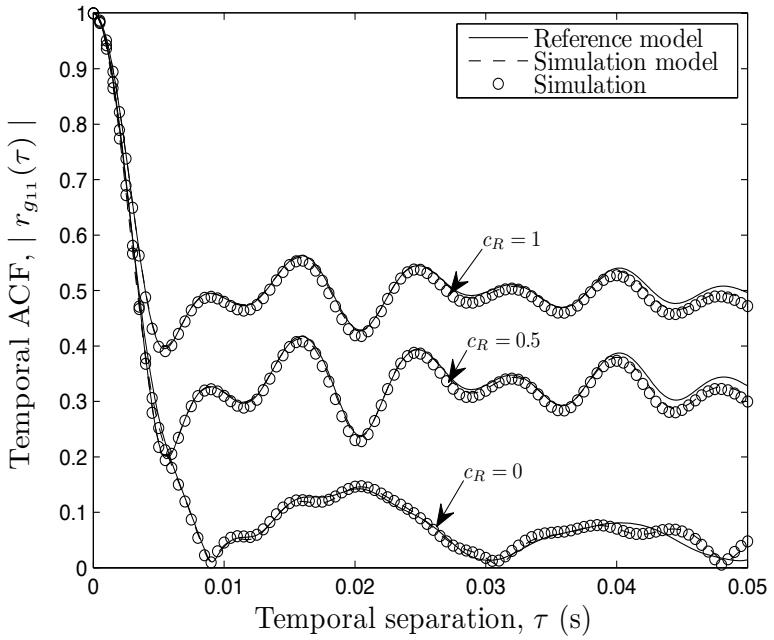

Figure C.2: Absolute values of the ACFs $|r_{g_{11}}(\tau)|$ (reference model) and $|\tilde{r}_{g_{11}}(\tau)|$ (simulation model) for different Rice factors ($c_R = \{0, 0.5, 1\}$, $R_1 = 14$ m, $R_2 = 8$ m, $x_T = 10$ m, $x_R = 12$ m, $y_T = 2$ m, and $y_R = 4$ m).

Fig. C.3 presents the temporal ACF $r_{g_{11}}(\tau)$ of the reference model given by (C.48) under certain geometrical conditions, which meet the geometry of the one-ring model [4, Eq. (9)], i.e., $R_1 = 14$ m, $R_2 = 0$ m, $x_T = 420$ m, $y_T = 0$ m, $x_R = 0$ m, and $y_R = 0$ m . A perfect fitting between the temporal ACF of the proposed reference model and that of the one-ring model can be observed in Fig. C.3, which validates

the usefulness of the proposed model and demonstrates that the proposed model includes the one-ring model as a special case.

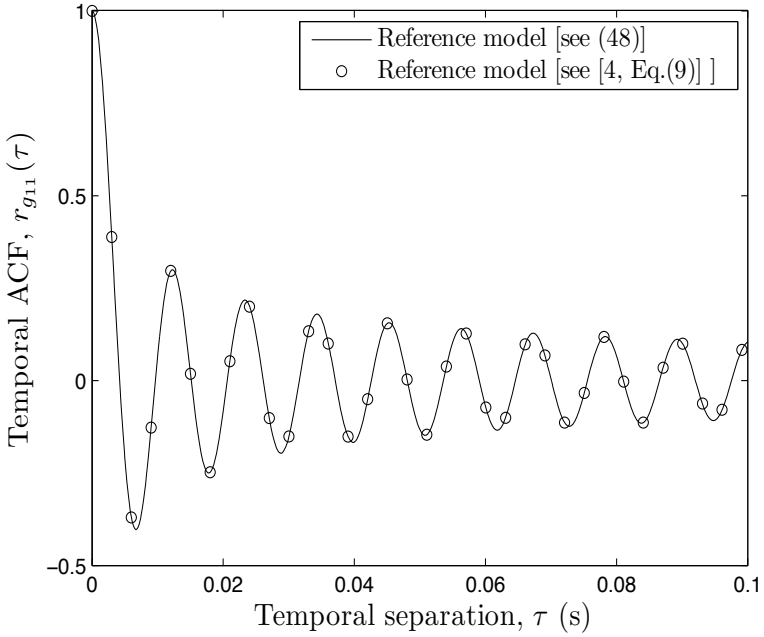

Figure C.3: Temporal ACF $r_{g_{11}}(\tau)$ of the reference model [see (C.48)] in comparison with the temporal ACF of the one-ring model [4, Eq. (9)] for a NLOS propagation scenario ($c_R = 0$, $R_1 = 14$ m, $R_2 = 0$ m, $x_T = 420$ m, $x_R = 0$ m, $y_T = 0$ m, and $y_R = 0$ m).

In Fig. C.4, the absolute value of the 2D space CCF $|\rho_{11,22}(\delta_T, \delta_R)|$ of the reference model is presented for a LOS propagation scenario ($c_R = 1$). The result has been obtained using (C.47). From Fig. C.4, we can realize that the complex channel gains $g_{kl}(t)$ and $g_{k'l'}(t)$ are highly correlated even for relatively large antenna element spacings.

VII. Conclusion

In this paper, a novel MIMO C2C channel model has been developed based on the geometrical curved street scattering model. By a combination of single- and double-bounce scattering components, we have analyzed the temporal ACF and the 2D space CCF of the reference model under both LOS and NLOS propagation conditions. To find a proper simulation model, the SOC principle has been applied. It has been shown that the SOC channel simulator approximates the reference model with respect to the temporal ACF with high accuracy. The usefulness of the proposed model has been validated by demonstrating a perfect fit between the ACF of

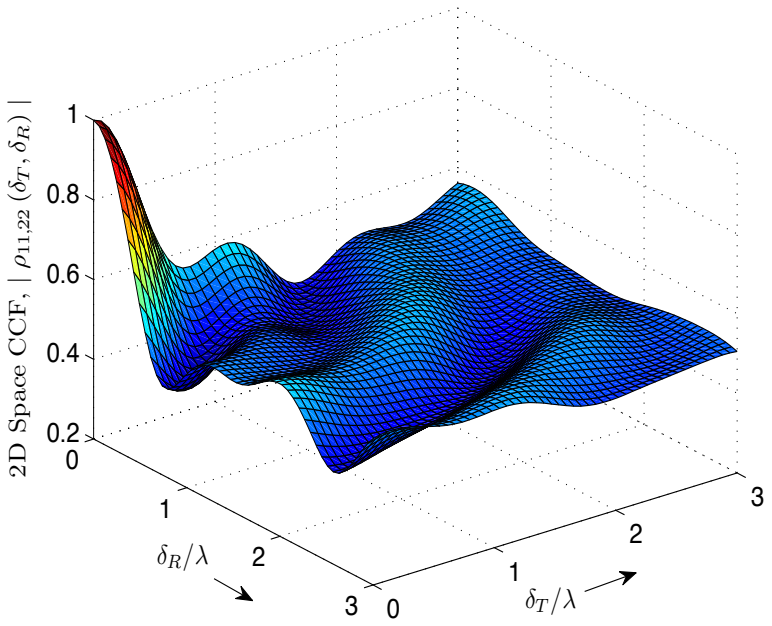

Figure C.4: Absolute value of the 2D space CCF $|\rho_{11,22}(\delta_T,\delta_R)|$ of the reference model for a LOS propagation scenario ($c_R = 1$, $R_1 = 14$ m, $R_2 = 8$ m, $x_T = 10$ m, $x_R = 12$ m, $y_T = 2$ m, and $y_R = 4$ m).

the reference model and that of the one-ring model. Further investigations focusing on the effect of moving scatterers on the statistics of MIMO C2C channels are planned in our future work.

REFERENCES

[1] ITS project, http://www.its.dot.gov/index.htm,, Nov. 2007.

[2] A. S. Akki and F. Haber, "A statistical model of mobile-to-mobile land communication channel," *IEEE Trans. Veh. Technol.*, vol. 35, no. 1, pp. 2–7, Feb. 1986.

[3] I. E. Telatar, "Capacity of multi-antenna Gaussian channels," *European Trans. Telecommun. Related Technol.*, vol. 10, no. 6, pp. 585–595, Nov./Dec. 1999.

[4] M. Pätzold and B. O. Hogstad, "A space-time channel simulator for MIMO channels based on the geometrical one-ring scattering model," in *Proc. 60th IEEE Semiannual Veh. Technol. Conf., VTC 2004-Fall. Los Angeles, CA, USA*, vol. 1, Sept. 2004, pp. 144–149.

[5] M. Pätzold, B. O. Hogstad, and N. Youssef, "Modeling, analysis, and simulation of MIMO mobile-to-mobile fading channels," *IEEE Trans. Wireless Commun.*, vol. 7, no. 2, pp. 510–520, Feb. 2008.

[6] A. G. Zajic and G. L. Stüber, "Space-time correlated mobile-to-mobile channels: modelling and simulation," *IEEE Trans. Veh. Technol.*, vol. 57, no. 2, pp. 715–726, Mar. 2008.

[7] M. Pätzold and B. O. Hogstad, "A wideband MIMO channel model derived from the geometrical elliptical scattering model," *Wireless Communications and Mobile Computing*, vol. 8, pp. 597–605, May 2008.

[8] H. Zhiyi, C. Wei, Z. Wei, M. Pätzold, and A. Chelli, "Modelling of MIMO vehicle-to-vehicle fading channels in T-junction scattering environments," in *Proc. 3rd European Conference on Antennas and Propagation, EuCAP 2009*. Berlin, Germany, Mar. 2009, pp. 652–656.

[9] N. Avazov and M. Pätzold, "A geometric street scattering channel model for car-to-car communication systems," in *Proc. International Conference on Advanced Technologies for Communications, ATC 2011*. Da Nang City, Vietnam, Aug. 2011, pp. 224–230.

[10] R. Wang and D. Cox, "Channel modeling for ad hoc mobile wireless networks," in *Proc. the 55th IEEE Veh. Technol. Conf., VTC 2002-Spring, Birmingham, AL*, vol. 1, May 2002, pp. 21 – 25.

[11] C. S. Patel, G. L. Stüber, and T. G. Pratt, "Simulation of Rayleigh-faded mobile-to-mobile communication channels," *IEEE Trans. Commun.*, vol. 53, no. 11, pp. 1876–1884, Nov. 2005.

[12] X. Cheng, C. X. Wang, D. I. Laurenson, S. Salous, and A. V. Vasilakos, "An adaptive geometry-based stochastic model for non-isotropic MIMO mobile-to-mobile channels," *IEEE Trans. Wireless Commun.*, vol. 8, no. 9, pp. 4824–4835, Sept. 2009.

[13] J. Maurer, T. Fügen, and W. Wiesbeck, "Narrow-band measurement and analysis of the inter-vehicle transmission channel at 5.2 ghz," in *Proc. 55th IEEE Veh. Technol. Conf., VTC 2002-Spring, Birmingham, AL*, vol. 3, May 2002, pp. 1274 – 1278.

[14] J. Kunish and J. Pamp, "Wideband car-to-car radio channel measurements and model at 5.9 GHz," in *Proc. 68th IEEE Veh. Technol. Conf., VTC 2008-Fall*, Sept. 2008, pp. 1–5.

[15] A. G. Zajic and G. L. Stüber, "A three-dimensional MIMO mobile-to-mobile channel model," Mar. 2007, pp. 1883–1887.

[16] ——, "A three-dimensional parametric model for wideband MIMO mobile-to-mobile channels," Nov. 2007, pp. 3760–3764.

[17] G. Morrish, *Street Design Guidelines*. Landcom Project., 2006, 41 pages.

[18] M. Nilsson, J. Slettenmark, and C. Beckman, "Wave propagation in curved road tunnels," in *IEEE Antennas and Propagation Society International Symposium, 1998*, vol. 4, June 1998, pp. 1876–1879.

[19] M. Pätzold, *Mobile Radio Channels*, 2nd ed. Chichester: John Wiley & Sons, 2011, 583 pages.

[20] A. Papoulis and S. U. Pillai, *Probability, Random Variables and Stochastic Processes*, 4th ed. New York: McGraw-Hill, 2002.

[21] M. Pätzold and B. Talha, "On the statistical properties of sum-of-cisoids-based mobile radio channel simulators," in *Proc. 10th International Symposium on Wireless Personal Multimedia Communications, WPMC 2007*. Jaipur, India, Dec. 2007, pp. 394–400.

[22] C. A. Gutiérrez and M. Pätzold, "The design of sum-of-cisoids Rayleigh fading channel simulators assuming non-isotropic scattering conditions," *IEEE Trans. Wireless Commun.*, vol. 9, no. 4, pp. 1308–1314, Apr. 2010.